Title	Nonhomogeneous-nonequilibrium two-phase-flow model for nuclear reactor single-channel stability
Author(s)	Zhao, Jiyun; Tso, Chih Ping; Tseng, King Jet
Citation	Zhao, J., Tso, C. P., & Tseng, K. J. (2012). Nonhomogeneous-nonequilibrium two-phase-flow model for nuclear reactor single-channel stability. Nuclear technology, 180(1), 78-88.
Date	2011
URL	http://hdl.handle.net/10220/18357
Rights	© 2011 American Nuclear Society, La Grange Park, Illinois. This paper was published in Nuclear technology and is made available as an electronic reprint (preprint) with permission of American Nuclear Society, La Grange Park, Illinois. The paper can be found at the following official URL: http://www.ans.org/pubs/journals/nt/a_14520. One print or electronic copy may be made for personal use only. Systematic or multiple reproduction, distribution to multiple locations via electronic or other means, duplication of any material in this paper for a fee or for commercial purposes, or modification of the content of the paper is prohibited and is subject to penalties under law.

NONHOMOGENEOUS-NONEQUILIBRIUM TWO-PHASE-FLOW MODEL FOR NUCLEAR REACTOR SINGLE-CHANNEL STABILITY ANALYSIS

THERMAL HYDRAULICS

KEYWORDS: *reactor stability, two-phase-flow models, stability map*

JIYUN ZHAO,[a]* C. P. TSO,[b] and K. J. TSENG[a]

[a]*EXQUISITUS, Centre for E-City, School of Electrical and Electronics Engineering, Nanyang Technological University, Singapore*
[b]*Nanyang Technological University, School of Mechanical and Aerospace Engineering, Division of Thermal and Fluids Engineering, Singapore*

Received July 12, 2011
Accepted for Publication December 12, 2011

The effects of two-phase-flow modeling on nuclear reactor single-channel stability analysis are investigated with four two-phase-flow models, namely, the homogeneous-equilibrium model, the homogeneous-nonequilibrium model, the nonhomogeneous-equilibrium model, and the nonhomogeneous-nonequilibrium model. The models are applied to hot-channel analyses of a proposed typical supercritical-water-cooled-reactor (SCWR) design. The neutral stability boundaries derived by using the four models are compared and plotted on the traditional subcooling number versus phase change number plane. To ensure proper development of the models, they are benchmarked to the experimental data. It is found that the homogeneous models predict more conservative stability boundaries than the nonhomogeneous models and that the differences of the stability boundaries predicted by all four two-phase-flow models are reduced under higher-pressure conditions.

I. INTRODUCTION

The single- or parallel-channel density wave oscillation (DWO) type of flow instability is a well-known and important issue in the design of boiling water reactors (BWRs), and such DWO flow instability needs to be avoided during actual operation. For the supercritical fluids proposed to be used in Generation IV supercritical-water-cooled reactors (SCWRs), although the coolant is normally under a single-phase supercritical pressure condition during steady-state operation, two-phase flow under subcritical pressure may occur during some off-normal conditions. Therefore, an appropriate two-phase-flow model also needs to be developed for SCWR stability analysis.

For a two-phase-flow channel, the governing parameters for flow stability are the subcooling number and the phase change number (also called the Zuber number). They were derived from nondimensional analyses of the conservation equations and are usually used to plot the stability map that defines the neutral boundary between stable and unstable regions on a plane.[1,2] Construction of stability maps for the flow inside a heated channel at subcritical pressure has a long history. Reference 1 uses a nonhomogeneous drift-flux model with a thermal equilibrium condition to construct a stability map in the subcooling number versus phase change number plane. Reference 3 improves the Ref. 1 model by including the effect of thermal nonequilibrium. But, deriving the characteristic equation analytically using a detailed vapor generation model such as an exponential distribution was found to be too complicated. The exponential distribution was simplified to a linear model in Ref. 3 so that the characteristic equation could be derived analytically.

More recently, Ref. 4 has compared the stability boundary effects of three different two-phase-flow models: homogeneous-equilibrium model (HEM), drift-flux

*E-mail: jyzhao@ntu.edu.sg

model, and two-fluid model. In Ref. 4, it is found that HEM is the most conservative among the three compared. Using a nonlinear reduced-order model, Ref. 5 investigated the effects of using a drift-flux model versus HEM in a nuclear-coupled thermal-hydraulic BWR stability analysis. It was found that HEM is not always more conservative than the drift-flux model.

In the case of the SCWR, although the supercritical water does not experience phase change, the thermodynamic properties exhibit boiling-like drastic changes around some pseudosaturation temperature. In analogy to subcritical water, nondimensional parameters called the pseudosubcooling number and the expansion number were derived for supercritical water channel stability.[2–6]

A three-region model consisting of a heavy fluid region, a heavy-light fluid mixture region, and a light fluid region was used to simulate the supercritical coolant flowing through the core, and a stability map was constructed in the pseudosubcooling number versus expansion number plane. Reference 7 also confirmed similar dynamic behavior between subcritical and supercritical water flow channels. HEM was used in simulating the heavy-light fluid mixture region.[2–6] To ensure that HEM is adequate in simulating supercritical water, one is required to compare it with other two-phase-flow models.

In the present work, we use nonhomogeneous and nonequilibrium models with a detailed exponential vapor generation distribution for two-phase flow, and we numerically derive the characteristic equation. To have a complete comparison and better understanding of the modeling effects of nonhomogeneity and nonequilibrium on the stability boundaries, we construct the stability maps using four different two-phase-flow models, namely, HEM, the homogeneous-nonequilibrium model (HNEM), the nonhomogeneous-equilibrium model (NHEM), and the nonhomogeneous-nonequilibrium model (NHNEM). The nonequilibrium models, HNEM and NHNEM, account for the existence of subcooled boiling, whereas the nonhomogeneous models, NHEM and NHNEM, incorporate the drift-flux concepts.

Extensive BWR experience shows that neutron reactivity feedback creates a fission power response to density perturbation, and that power is filtered through the fuel rods, causing a time lag for the heat flux that counteracts the original perturbation of the fluid density. The heat conduction delay—even though the gain is attenuating—forces the feedback to be destabilizing. In this paper, an idealized model without coupling the power fluctuations is used. Since the main purpose of this paper is to compare the aforementioned four different two-phase-flow models, this simplification in modeling will not hurt the comparative value of this paper. The impact of neutronic feedback and power fluctuation will be investigated in future work.

II. MODEL DEVELOPMENT

II.A. NHNEM Description

II.A.1. Net Vapor Generation Point and Exponential Vapor Generation Rate

The net vapor generation point that defines the boiling boundary was predicted by applying the widely used Saha and Zuber correlation[3]:

$$\Delta h_\lambda = h_f - h_\lambda = 0.0022 \frac{q_w'' D_h C_{pf}}{k_f} \quad , \quad P_e \le 70\,000 \tag{1}$$

and

$$\Delta h_\lambda = h_f - h_\lambda = 154 \frac{q_w''}{\rho_f u_{in}} \quad , \quad P_e \ge 70\,000 \ . \tag{2}$$

For the vapor generation rate, an exponential distribution[3] along the channel is assumed:

$$\Gamma_g = \frac{q_w'' P_h}{A_c h_{fg}} \left[1 - \exp\left(- \frac{z - \lambda_1(t)}{\Delta l} \right) \right]$$

$$= \Gamma_{g,eq} \left[1 - \exp\left(- \frac{z - \lambda_1(t)}{\Delta l} \right) \right] \ , \tag{3}$$

where

$$\lambda_1 = \frac{G A_c (h_\lambda - h_{in})}{q_w'' P_h} = \text{boiling boundary} \tag{4}$$

and

$$\Delta l = \lambda_{eq} - \lambda_1$$

$$= \frac{G A_c (h_f - h_\lambda)}{q_w'' P_h} = \text{characteristic length} \ . \tag{5}$$

The vapor generation rate model based on the exponential distribution and the thermal equilibrium assumption is illustrated in Fig. 1.

II.A.2. Bestion Drift-Flux Correlation

For NHEM and NHNEM, the Bestion's drift-flux correlation[8] is applied in this work. According to Ref. 9, despite the simplicity of this correlation, it yields good

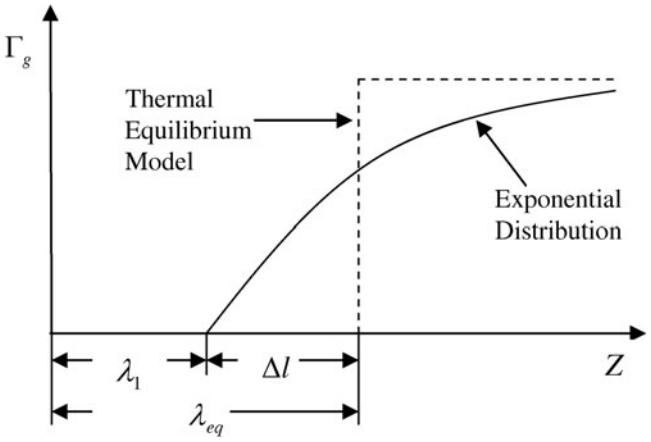

Fig. 1. Comparison of two vapor generation models.

results for most of the experimental data. This correlation has the following form:

$$C_o = 1.0$$

and

$$V_{gh} = 0.188\sqrt{\frac{gD_e\Delta\rho}{\rho_g}} \quad , \tag{6}$$

where

C_o = concentration parameter and represents the global effect due to radial nonuniform void and velocity profiles

V_{gj} = drift velocity of the vapor.

II.A.3. Subcooled Flow Quality and Void Fraction

Using the exponential vapor generation model defined in Eq. (3), Ref. 3 derives the flow quality in the following form:

$$x(z) = x_{eq} - x_{eq,\lambda}\exp\left(\frac{x_{eq}}{x_{eq,\lambda}} - 1\right) \quad . \tag{7}$$

Formula (7) follows that of Ref. 10 using the profile-fit approach. The equilibrium quality in formula (7) can be expressed as

$$x_{eq} = \frac{q''_w P_h \Delta l}{GA_c h_{fg}}\left(\frac{z-\lambda_1}{\Delta l} - 1\right) \quad . \tag{8}$$

The value $x_{eq,\lambda}$ is the equilibrium quality at net vapor generation point $z = \lambda_1$. The void fraction may then be predicted from the drift-flux model as

$$\alpha(z) = \frac{x}{C_o\left(x\frac{\Delta\rho}{\rho_f} + \frac{\rho_g}{\rho_f}\right) + \frac{\rho_g V_{gj}}{G}} \quad . \tag{9}$$

II.B. Friction Factors

According to Ref. 11, for $\mathrm{Re} = 3\times10^4$ to 3×10^6, the following McAdams relation can be applied:

$$f = 0.184\mathrm{Re}^{-0.2} \quad . \tag{10}$$

For $\mathrm{Re} < 3\times10^4$, the following Blasius relation can be applied:

$$f = 0.316\mathrm{Re}^{-0.25} \quad . \tag{11}$$

Using the above correlations [Eqs. (10) and (11)], the friction factor calculations are carried out as follows:

1. *Single-phase liquid region*: The friction factor is assumed constant and equals f_s, which is the friction factor at the boiling boundary. Thus, $f_1 = f_s$.

2. *Two-phase mixture flow region*: According to Ref. 1, in the two-phase mixture region, the friction factor could be assumed in the following form:

$$f_2 = C_m f_s \quad , \tag{12}$$

where C_m is a constant number and f_s is calculated at the boiling boundary. For high system pressure and reasonably high exit qualities in a subcritical pressure system, C_m has a range from 1.5 to 2.5. Thus, $C_m = 2.0$ was taken in both Refs. 1 and 3. In this paper, $C_m = 2.0$ is also taken. Thus, $f_2 = 2.0 f_s$.

It is worth noting that single-phase friction as a function of the Reynolds number given in Eqs. (10) and (11) is discontinuous, which can greatly disturb the stability analysis. In this paper, since the saturation properties are used to calculate the friction factor that is assumed to be constant along the channel in the specific single- or two-phase-flow regions, only one correlation, either Eq. (10) or Eq. (11), is used for a specific analysis case. For any stability analysis, the discontinuity issue must be resolved if the two correlations are both used along the flow channel in a specific analysis case.

II.C. Characteristic Equation for NHNEM

The two-phase-flow models described above are used in this section to develop the stability characteristic equation for a typical SCWR hot channel. Further details can be found in Refs. 2 and 6.

The single flow channel of the SCWR core in the subcritical pressure condition can be divided into four

sections: the inlet orifice, the lower nonheated part, the heated part, and the upper nonheated part.

II.C.1. Inlet Orifice

The momentum equation for the inlet orifice can be expressed as

$$\Delta p_{ori} = k_{in} \frac{\rho_f u_{in}^2}{2} \quad . \tag{13}$$

Perturbation and Laplace transformation of Eq. (13) yields

$$\delta \Delta p_{ori} = k_{in} \rho_f u_{in} \delta u_{in} \quad . \tag{14}$$

II.C.2. Heated Part

This part includes the single-phase liquid region and the two-phase mixture region.

II.C.2.a. Liquid Region. The conservation equations can be expressed as

$$\frac{\partial u}{\partial z} = 0 (\rho(z) = \rho_f = Const.) \quad , \tag{15}$$

$$\rho_f \frac{\partial h}{\partial t} + \rho_f u_{in} \frac{\partial h}{\partial z} = \frac{q'' P_h}{A_c} \quad , \tag{16}$$

and

$$-\frac{\partial \rho}{\partial z} = \rho_f \frac{du_{in}}{dt} + \frac{f_1 \rho_f u_{in}^2}{2D_e} + \rho_f g \quad . \tag{17}$$

In this region, the water density is assumed constant and equal to the saturated water density ρ_f. Perturbing and Laplace transforming energy equation (16), one obtains

$$\frac{d\delta h}{dz} + \frac{s}{u_{in}} \delta h + \frac{q'' P_h}{A_c \rho_f u_{in}^2} \delta u_{in} = 0 \quad . \tag{18}$$

Equation (18) is a Bernoulli-type ordinary differential equation that can be readily integrated from inlet to some axial point z. Then, the enthalpy perturbation at the net vapor generation location is

$$\delta h(s, \lambda_1) = \exp(-s\lambda_1 / u_{in}) \delta h_{in} - \frac{q'' P_h}{\rho_f u_{in} A_c s} \times [1 - \exp(-s\lambda_1 / u_{in})] \delta u_{in} \quad . \tag{19}$$

For perturbation of the boiling boundary, there are two parts. The first part is due to the direct relationship of the inlet velocity to the enthalpy at the point of net vapor generation, which may be obtained from Saha-Zuber formulas (1) and (2) as

$$\delta h_1(s, \lambda_1) = \begin{cases} 0 \quad , & P_e \le 70\,000 \\ 154 \dfrac{q''_w}{\rho_f u_{in}^2} \delta u_{in} \quad , & P_e \ge 70\,000 \quad . \end{cases} \tag{20}$$

The other part is due to the influence of inlet velocity oscillation on the enthalpy at the boiling boundary or point of net vapor generation, which can be described as follows:

$$\delta h_2(s, \lambda_1) = -\frac{q'' P_h}{\rho_f u_{in} A_c s} [1 - \exp(-s\lambda_1 / u_{in})] \delta u_{in} \quad . \tag{21}$$

Then, the total enthalpy oscillation at the net vapor generation point is

$$\delta h(s, \lambda_1) = \delta h_1(s, \lambda_1) + \delta h_2(s, \lambda_1) \quad .$$

Thus, the boiling boundary perturbation can be obtained as the following. For Pe $\le$ 70 000,

$$\delta \lambda_1 = -\frac{\rho_f A_c u_{in}}{q'' P_h} \delta h(s, \lambda_1) = \frac{1 - \exp(-s\lambda_1 / u_{in})}{s} \delta u_{in} \quad . \tag{22}$$

For Pe $\ge$ 70 000,

$$\delta \lambda_1 = \left(154 \frac{A_c}{P_h u_{in}} + \frac{1 - \exp(-s\lambda_1 / u_{in})}{s} \right) \delta u_{in} \quad . \tag{23}$$

The authors of Ref. 3 and 12 found that the boiling boundary fluctuation model described by Eq. (22) was a better match to the experimental data for flow instability even for Pe $\ge$ 70 000. Thus, Eq. (22) will be applied during this analysis for all Peclet numbers. If the inlet enthalpy h_{in} in Eq. (4) is higher than h_λ, the net vapor generation will occur right at the inlet of the channel. In that case, $\lambda_1 = 0$ and $\delta \lambda_1 = 0$.

From integration of the momentum equation, the pressure drop perturbation in this region can be obtained as

$$\delta(\Delta p_{liquid}) = \Gamma_1 \delta u_{in} + \Gamma_2 \delta h_{in} \quad , \tag{24}$$

where

$$\Gamma_1 = \rho_f \lambda_1 s + \frac{f_1 \rho_f u_{in} \lambda_1}{D_e} + \left(\frac{f_1 \rho_f u_{in}^2}{2D_e} + \rho_f g \right) \times \left(\frac{1 - \exp(-s\lambda_1 / u_{in})}{s} \right) \quad . \tag{25}$$

Since we assume no inlet enthalpy fluctuation, the derivation of Γ_2 is omitted.

II.C.2.b. Two-Phase Mixture Region. This region starts from the net vapor generation point. The conservation equations for two-phase flow provided in Ref. 12 are applied:

$$\frac{\partial j}{\partial z} = \frac{\Gamma_g \Delta\rho}{\rho_g \rho_f} \ , \tag{26}$$

$$\frac{\partial \rho_m}{\partial t} + C_k \frac{\partial \rho_m}{\partial z} + \rho_m \frac{\Gamma_g \Delta\rho}{\rho_g \rho_f} = 0 \ , \tag{27}$$

$$\rho_m \left(\frac{\partial u_m}{\partial t} + u_m \frac{\partial u_m}{\partial z} \right) = -\frac{\partial p_m}{\partial z} - \frac{f_m}{2D_e} \rho_m u_m^2 - g\rho_m - \frac{\partial}{\partial z} \left[\frac{\rho_f - \rho_m}{\rho_m - \rho_g} \frac{\rho_f \rho_g}{\rho_m} V_{gj}^2 \right] \ , \tag{28}$$

and

$$\rho_m \left(\frac{\partial h_m}{\partial t} + u_m \frac{\partial h_m}{\partial z} \right) = \frac{q_w'' P_h}{A_c} + \frac{\partial p_m}{\partial t} - \frac{\partial}{\partial z} \left(\frac{\rho_f - \rho_m}{\rho_m} \frac{\rho_f \rho_g}{\Delta\rho} V_{gj} h_{fg} \right) \ , \tag{29}$$

where

$$C_k = j + V_{gj} \ , \tag{30}$$

$$u_m = j - \left(\frac{\rho_f}{\rho_m} - 1 \right) V_{gj} \ , \tag{31}$$

$$\rho_m = (1 - \alpha)\rho_f + \alpha\rho_g \ , \tag{32}$$

and

$$h_m = \frac{\alpha\rho_g}{\rho_m} h_g + \frac{(1 - \alpha)\rho_f}{\rho_m} h_f \ . \tag{33}$$

For the numerical characteristic equation derivation, this region is divided into N nodes. Conservation equations (26) through (33) are linearized, perturbed, and Laplace transformed. The pressure drop oscillation at every node i is obtained by applying conservation equations (26) through (33), and the total pressure drop oscillation across this region is obtained by adding up the oscillations of every node.

Linearization, perturbation, and Laplace transformation of velocity equation (26) at node i yield

$$\delta j_{i+1} = \delta j_i + \frac{\Delta z \Delta\rho}{\rho_g \rho_f} \delta\Gamma_{g,i} \ . \tag{34}$$

The volumetric flux oscillation at the first node ($z = \lambda_1$) should be the same as the inlet velocity oscillation. Therefore, $\delta j_1 = \delta u_{in}$.

From Eq. (3),

$$\delta\Gamma_{g,i} = -\Gamma_{g,eq} \exp\left(-\frac{(i-1)\Delta z}{\Delta l} \right) \frac{1}{\Delta l} \delta\lambda_1 \ . \tag{35}$$

Linearization, perturbation, and Laplace transformation of density propagation equation (27) at node i yield

$$\delta\rho_{m,i+1} = -\frac{\Delta z}{j_i + V_{gj}} \left(s + \frac{j_{i+1} - 2j_i - V_{gi}}{\Delta z} \right) \delta\rho_{m,i} - \frac{\rho_{m,i+1} - \rho_{m,i}}{j_i + V_{gj}} \delta j_i - \frac{\Delta z}{j_i + V_{gj}} \frac{\rho_{m,i} \Delta\rho}{\rho_g \rho_f} \delta\Gamma_{g,i} \ . \tag{36}$$

The density oscillation at the first node ($z = \lambda_1$) should be zero since the exponential vapor generation rate distribution will give a zero vapor generation rate at the boiling boundary.

Perturbation and Laplace transformation of identity (31) at node i yield

$$\delta u_{m,i} = \delta j_i + \frac{\rho_f V_{gj}}{\rho_{m,i}^2} \delta\rho_{m,i} \ . \tag{37}$$

Now, we are ready for linearization, perturbation, and Laplace transformation of momentum equation (28) at node i. The acceleration part of the momentum equation is only related to the inlet and outlet conditions of the region, and it is treated separately:

$$\delta\Delta p_i = \rho_{m,i} u_{m,i} \delta u_{m,i+1} + (u_{m,i}(u_{m,i+1} - u_{m,i}) + f_2 \Delta z u_{m,i}/(2D_e) + 9.81\Delta z)\delta\rho_{m,i} + (s\rho_{m,i}\Delta z + \rho_{m,i}(u_{m,i+1} - u_{m,}) - \rho_{m,i} u_{m,i} + f_2 \Delta z \rho_{m,i} u_{m,i}/D_e)\delta u_{m,i} \ . \tag{38}$$

For the acceleration part,

$$\Delta p_{acc} = \int_{\lambda_1+\delta\lambda_1}^{L} \frac{\partial}{\partial z}\left(\frac{\rho_f-\rho_m}{\rho_m-\rho_g}\frac{\rho_f\rho_g}{\rho_m}V_{gj}^2\right)dz$$

$$= \frac{\rho_f-\rho_m(L)}{\rho_m(L)-\rho_g}\frac{\rho_f\rho_g}{\rho_m(L)}V_{gj}^2$$

$$\approx \frac{\rho_f-\rho_m(L)}{\rho_m(L)}\frac{\rho_f\rho_g}{\rho_m(L)}V_{gj}^2 \quad . \tag{39}$$

It is easy to perturb and Laplace transform Eq. (39) to obtain the total acceleration pressure drop oscillation as

$$\delta\Delta p_{acc} = \frac{\rho_m(L)-2\rho_f}{\rho_m^3(L)}\rho_f\rho_g V_{gj}^2\delta\rho_m(L) \quad . \tag{40}$$

The nodalization is from λ_1 to L, but the real case should be from $\lambda_1 + \delta\lambda_1$ to L. Thus, the pressure drop oscillation due to boiling boundary oscillation should be deleted from the total oscillation. The pressure drop oscillation due to boundary oscillation can be expressed as

$$\delta\Delta p_{\delta\lambda_1} = \left(G\left.\frac{\partial u_m}{\partial z}\right|_{z=\lambda_1} + f_2\rho_f u_{in}^2/(2D_e) + 9.81\rho_f\right)\delta\lambda_1 \quad . \tag{41}$$

From identity equation (31),

$$u_m = j - \left(\frac{\rho_f u_m}{G} - 1\right)V_{gj} = j - \left(\frac{\rho_f u_m}{\rho_f u_{in}} - 1\right)V_{gj}$$

$$= j - \left(\frac{u_m}{u_{in}} - 1\right)V_{gj} \quad . \tag{42}$$

Solving u_m from formula (42),

$$u_m = \frac{j + V_{gj}}{1 + \dfrac{V_{gj}}{u_{in}}} \quad . \tag{43}$$

Thus,

$$\frac{\partial u_m}{\partial z} = \frac{\partial j}{\partial z}\frac{u_{in}}{u_{in}+V_{gj}} = \frac{\Gamma_g\Delta\rho}{\rho_g\rho_f}\frac{u_{in}}{u_{in}+V_{gj}} \quad . \tag{44}$$

For the exponential vapor generation distribution, $\Gamma_g = 0.0$ at $z = \lambda_1$. Therefore, $(\partial u_m/\partial z)|_{z=\lambda_1} = 0.0$. Thus,

$$\delta\Delta p_{\delta\lambda_1} = (f_2\rho_f u_{in}^2/(2D_e) + 9.81\rho_f)\delta\lambda_1 \quad . \tag{45}$$

Now, the total pressure drop oscillation in the heated part can be expressed as

$$\delta\Delta p_{heated} = \delta\Delta p_{liquid} + \sum_{i=1}^{N}\delta\Delta p_i + \delta\Delta p_{acc} - \delta\Delta p_{\delta\lambda_1} \quad . \tag{46}$$

II.C.3. Nonheated Gas Plenum Part

II.C.3.a. Lower Gas Plenum. As mentioned in the supercritical region characteristic equation derivation, applying the conservation equations and assuming a constant density in this part, the relation between the pressure drop oscillation and the inlet flow oscillation can be expressed as

$$\delta\Delta p_{nod} = (f_1/D_e L_{nod}G + s\rho_f L_{nod})\delta u_{in} \quad . \tag{47}$$

II.C.3.b. Upper Gas Plenum. Applying the conservation equations to this part,

$$\delta\Delta p_{nou} = \left(f_2/D_e L_{nou}\frac{u_{m,n+1}^2}{2} + gL_{nou} + su_{m,n+1}L_{nou}\right)$$

$$\times\,\delta\rho_{m,n+1} + (f_2/D_e L_{nou}G + s\rho_{m,n+1}L_{nou})$$

$$\times\,\delta u_{m,n+1} \quad . \tag{48}$$

II.C.4. Total Pressure Drop Oscillation

Adding up all of above pressure drop oscillation parts, the total pressure drop oscillations can be obtained as

$$\delta\Delta p_{Channel} = \delta\Delta p_{ori} + \delta\Delta p_{heated} + \delta\Delta p_{nou} + \delta\Delta p_{nod} \quad . \tag{49}$$

If we set the drift velocity $V_{gj} = 0.0$, the characteristic equation, derived for NHNEM, will become that for the HNEM.

II.D. The Characteristic Equation for NHEM

The characteristic equation based on NHEM has been analytically derived in Ref. 1. In this paper, we derive the characteristic equation based on a numerical method since that for the NHNEM was derived numerically. Also, the numerical method avoids the complicated integration procedure that is needed in the analytical method.

The same procedure as adopted for NHNEM can be applied to NHEM. The vapor generation rate of exponential distribution needs to be changed to a constant value corresponding to the equilibrium vapor generation rate $\Gamma_{g,eq}$, which is defined in Eq. (3). Also, the two-phase region will start at $z = \lambda_{eq}$. Therefore, volumetric flux conservation equation (26) can be expressed as

$$\frac{\partial j}{\partial z} = \frac{\Gamma_g \Delta\rho}{\rho_g \rho_f} = \frac{\Gamma_{eg} \Delta\rho}{\rho_g \rho_f} = \frac{v_{fg}}{h_{fg}} \frac{q''_w P_h}{A_c} = \Omega_1 \ , \quad (50)$$

$$j(z) = u_{in} + \Omega_1 (z - \lambda_{eq}) \ , \quad (51)$$

and

$$\delta j = \delta u_{in} - \Omega_1 \delta\lambda_{eq} \ . \quad (52)$$

Therefore, the perturbation of volumetric flux will be constant along the channel in the two-phase region.

The density oscillation and mixture velocity oscillation will have the same scheme as NHNEM. However, the density oscillation of the boiling boundary for NHEM will be different from that of NHNEM since the vapor generation rate at the boiling boundary is not zero for NHEM while it is zero for NHNEM. According to Ref. 3, the density oscillation at the boiling boundary for NHEM can be derived as

$$\delta\rho_{m,1} = \frac{\rho_f \Omega_1}{u_{in} + V_{gj}} \delta\lambda_{eq} \ . \quad (53)$$

The pressure drop oscillation scheme will also be the same as NHNEM. Applying the same procedure as NHNEM, the characteristic equation based on NHEM can be derived easily. Similarly, if we set the drift velocity $V_{gj} = 0.0$, the characteristic equation, derived for NHEM, will become that for HEM.

III. COMPARISON OF DIFFERENT TWO-PHASE-FLOW MODELS

Using the four two-phase-flow models—HEM, HNEM, NHEM, and NHNEM—developed in Secs. II.C and II.D, the stability maps are plotted in the subcooling number versus phase change number plane.[1,13] The subcooling number is defined as

$$N_{sub} = \frac{(h_f - h_{in})}{h_{fg}} \frac{\Delta\rho}{\rho_g} \ . \quad (54)$$

The subcooling number scales the inlet subcooling and is the dimensionless residence time of a fluid particle in the single-phase liquid region. The phase change number scales the rate of phase change due to heat addition and is defined as

$$N_{pch} = \frac{v_{fg}}{h_{fg}} \frac{q'' P_h}{A_c} \frac{L}{u_{in}} \ . \quad (55)$$

For the previously mentioned typical SCWR design, stability boundaries are plotted at the pressure of 5.0 MPa for the hot channel (with $k_{in} = 20.0$). Figure 2 compares the four two-phase-flow models. Detailed information on the typical SCWR design that is required to conduct this analysis can be found in Ref. 14.

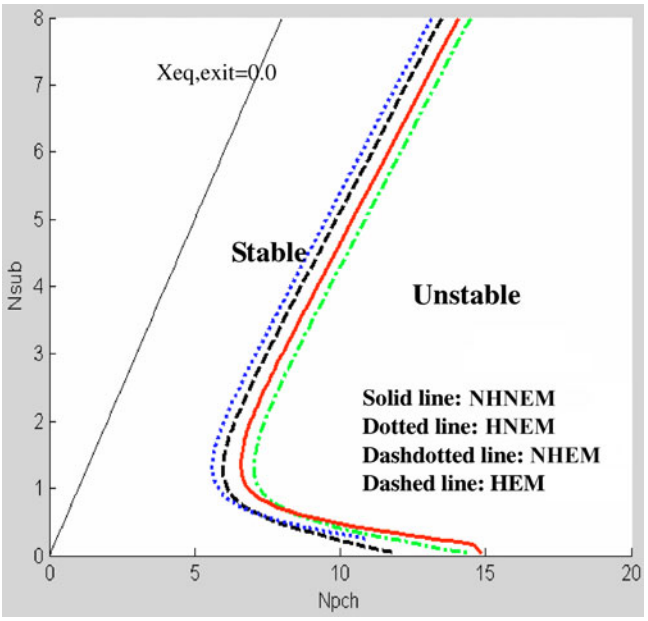

Fig. 2. Comparison of stability boundaries using the four different two-phase-flow models at 5.0 MPa.

Figure 2 indicates that HNEM predicts the most conservative stability boundary at high subcooling numbers, whereas HEM yields the most conservative stability boundary at low subcooling numbers. HEM and HNEM predict a more conservative stability boundary both for thermal equilibrium and thermal nonequilibrium conditions. This can be explained physically because in NHEM and NHNEM, the vapor phase always moves faster than the liquid phase. Thus, HEM and HNEM always calculate a higher void faction and a less stable system compared to NHEM and NHNEM. Therefore, HEM and HNEM predict a conservative stability boundary. On the other hand, at high subcooling numbers, HNEM and NHNEM are found to be more conservative than NHEM and HEM for all models: HEM, HNEM, NHEM, and NHNEM. Physically, HNEM and NHNEM predict a higher void fraction since the subcooled boiling was accounted for in HNEM and NHNEM. However, at low subcooling numbers, the situation reverses: HEM and NHEM predict a conservative boundary. This can also be explained physically. At low subcooling numbers, the subcooled boiling is negligible compared to the saturation boiling. Thus, HNEM and NHNEM do not affect the void fraction calculation much. But, at the saturation boiling region, HNEM and NHNEM with exponential vapor generation asymptotically approach HEM and NHEM, which makes the vapor generation rate of HNEM and NHNEM below that of HEM and NHEM. Therefore, the average void fraction for HNEM and NHNEM is less than that of HEM and NHEM as the inlet subcooling number is below some value.

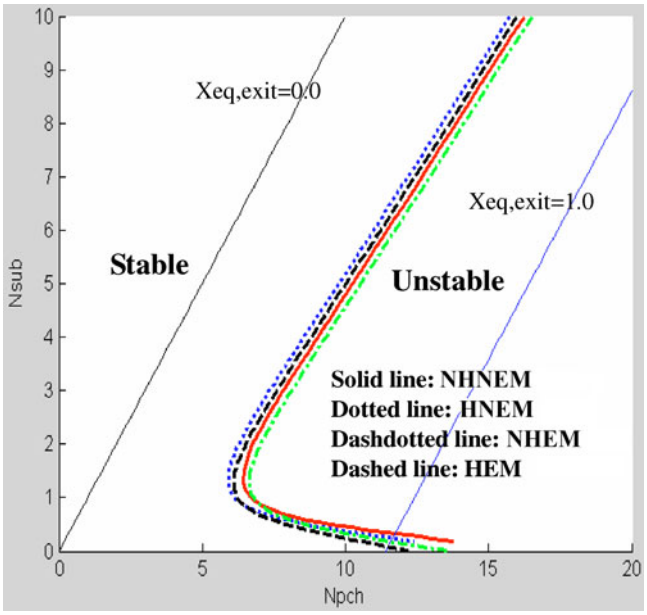

Fig. 3. Comparison of the four two-phase flow models at 10.0 MPa.

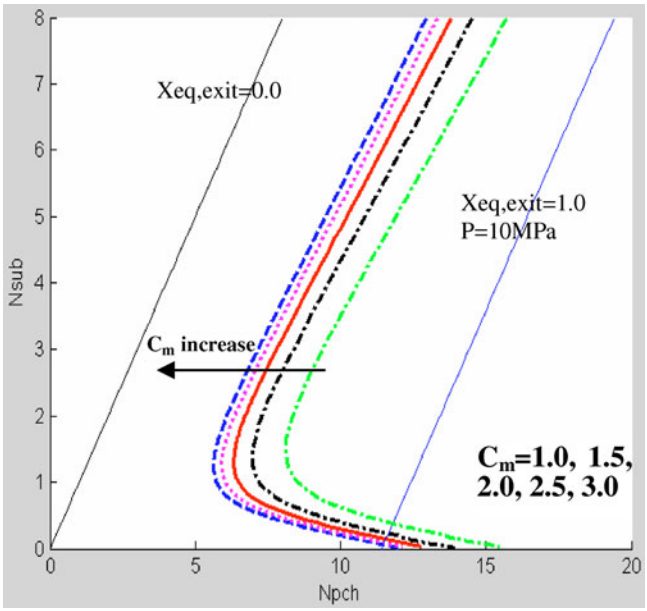

Fig. 4. Multiplier C_m effects on stability boundary.

Physically, the stability boundary differences among the four different models will decrease as the pressure increases. This can be seen from Fig. 3 where various stability boundaries have been plotted at a pressure of 10 MPa for the hot channel.

Therefore, at high pressures, simple HEM may be chosen for a quick check of the system stability boundary.

As mentioned previously, the value of multiplier C_m in the two-phase friction factor was assumed to be 2.0. The effect of C_m on the stability boundary was evaluated by setting $C_m = 1.0, 1.5, 2.0, 2.5, 3.0$ for HEM for the hot channel at 10-MPa pressure. The results are shown in Fig. 4.

Figure 4 indicates that the stability boundary will move toward the left as C_m increases. The effects on the stability boundary will decrease as C_m increases. Also, it is seen that applying $C_m = 2.0$ will give reasonable results since C_m ranges from 1.5 to 2.5. It is worth noting that although a constant two-phase friction factor multiplier is used in this paper—which will not hurt the comparative value of the paper, especially since a sensitivity study on the multiplier has been performed and a suitable value was chosen—the multiplier has strong dependence on steam quality. To evaluate the channel stability more accurately, a quality-dependent multiplier should be used.

IV. MODEL EVALUATION

To ensure the proper development of the models, the two-phase-flow models developed in this paper are compared with the experimental data of Refs. 15 and 16. The experiments of both Refs. 15 and 16 use water as the working fluid. Reference 15 uses an annulus as the heated channel with water at 70-atm pressure, whereas Ref. 16 uses a circular tube as the heated channel with water at 80-atm pressure.

The nonequilibrium models developed in this paper, HNEM and NHNEM, are compared with the experimental data in Figs. 5 and 6. It is seen that HNEM and NHNEM match the experimental data reasonably well.

The two experiments shown in Figs. 5 and 6 are also used in Ref. 1 to benchmark NHEM developed analytically. The comparison is shown in Figs. 25 and 27 of Ref. 1. To make sure HEM, HNEM, NHEM, and NHNEM are correctly developed, NHEM, developed numerically in this paper, is also plotted in Figs. 5 and 6. Comparing Figs. 25 and 27 in Ref. 1 with Figs. 5 and 6 in this paper, one can see that NHEM is consistent with the analytical model developed in Ref. 1, and therefore, the correctness of NHEM can be confirmed.

Figure 4 indicates that the stability boundary is sensitive to the two-phase friction factor C_m. As discussed previously, a value of $C_m = 2.0$ is chosen in this paper. To make sure a correct C_m value was selected, the NHNEM is evaluated against the experimental data by varying C_m. The results are shown in Figs. 7 and 8.

One can see from Figs. 7 and 8 that as Fig. 4 shows, the stability boundary is sensitive to the two-phase friction factor C_m and NHNEM matches the experimental data well as $C_m = 2.0$. In practice, a higher C_m value can be selected for conservatism.

One can see from Figs. 5 through 8 that the inversion of the stability boundary at low subcooling numbers and

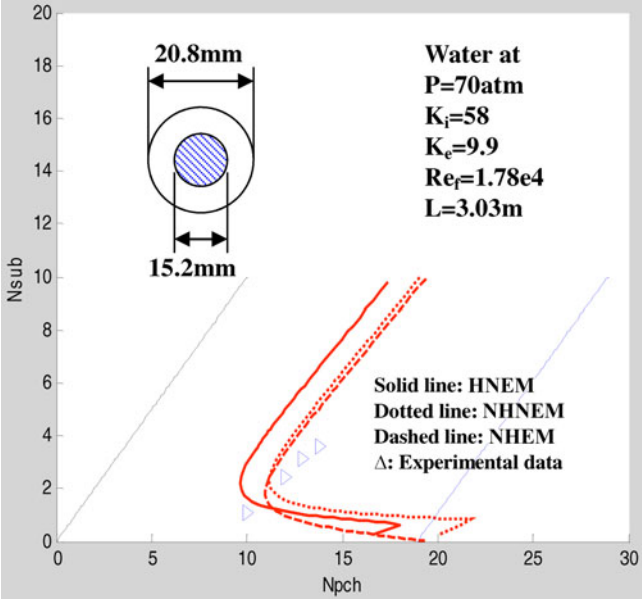

Fig. 5. Model evaluation with experimental data of Ref. 15.

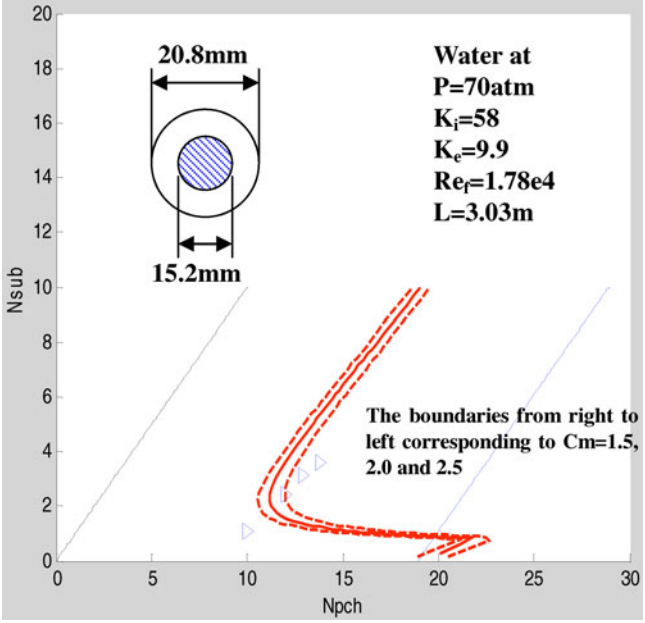

Fig. 7. The C_m effects on NHNEM with the experimental data of Ref. 15.

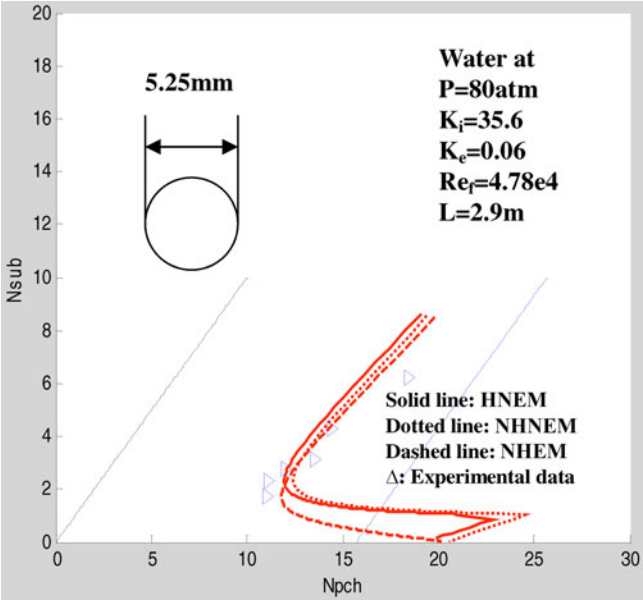

Fig. 6. Model evaluation with experimental data of Ref. 16.

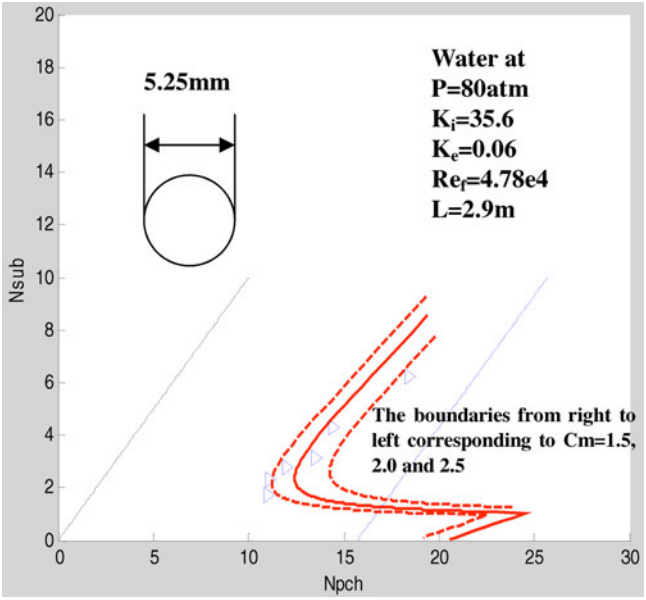

Fig. 8. The C_m effects on NHNEM with the experimental data of Ref. 16.

high phase change numbers occurs for HNEM and NHNEM. Further investigations on this phenomenon are required.

The experimental data used in evaluating HEM, HNEM, NHEM, and NHNEM in Figs. 5 through 8 are located in the region of stabilizing with increasing the subcooling number, i.e., the upper part of the stability map. Although the proposed SCWR is designed to operate in the upper part of the stability map for steady-state and sliding pressure start-up operation,[2,6] further investigation and model evaluation are required for the lower part of the stability map especially for the unusual stability boundary inversion phenomenon mentioned earlier.

V. CONCLUSIONS

Through the comparison of stability boundaries constructed using the four different two-phase-flow models, it was found that the homogeneous models, either equilibrium or nonequilibrium, i.e., HEM and HNEM, predict more conservative stability boundaries than the nonhomogeneous models, i.e., NHEM and NHNEM. The nonequilibrium models HNEM and NHNEM are found to be more conservative than the equilibrium models HEM and NHEM at high subcooling numbers, while the equilibrium models HEM and NHEM are more conservative than the nonequilibrium models HNEM and NHNEM at low subcooling numbers. Therefore, generally speaking, among the four different two-phase-flow models, HNEM predicts the most conservative stability boundary at high subcooling numbers, whereas HEM yields the most conservative stability boundary at low subcooling numbers.

In addition, investigation on the system pressure effects on the stability boundaries finds that the differences among the four stability boundaries are decreased as the system pressure increases. Therefore, HEM can be conveniently used with adequate accuracy to check the reactor flow stability at high-pressure operating conditions.

Finally, it is found that the stability boundary is sensitive to the two-phase friction factor C_m and that NHNEM is well-matched with the experimental data at $C_m = 2.0$. In practice, a higher C_m value can be selected for conservatism.

NOMENCLATURE

A_c = channel flow area (m^2)

C_k = kinematic wave velocity, $C_k = j + V_{gj}$ (m/s)

C_o = void distribution parameter

c_p = specific heat at constant pressure [kJ/(kg·K)]

D_e = hydraulic diameter (m)

f_1 = friction factor at liquid region

f_2 = friction factor at two-phase mixture region

f_s = friction factor at boiling boundary

G = mass flux ($kg/m^2 \cdot s$)

h = enthalpy (kJ/kg)

j = volumetric flux density (m/s)

K_{in} = inlet orifice coefficient

k_f = liquid thermal conductivity [W/(m·K)]

L = length of fuel rod heated region or channel heated length in the definition of phase change number (m)

L_{nod} = length of fuel rod lower gas plenum (m)

L_{nou} = length of fuel rod upper gas plenum (m)

N_{pch} = phase change number

N_{sub} = subcooling number

P_e = Peclet number, $P_e = \dfrac{GD_e c_{pf}}{k_f}$

P_h = heated perimeter (m)

p = pressure (MPa)

q'' (q''_w) = surface heat flux (kW/m^2)

Re = Reynolds number

s = variable of Laplace transformation

t = time (s)

u = coolant velocity (m/s)

V_{gj} = vapor drift velocity (m/s)

x = flow quality

x_{eq} = equilibrium quality

$x_{eq,exit}$ = equilibrium quality at channel exit

Greek

α = vapor void fraction

Γ = transfer function

Γ_g = actual vapor generation rate ($kg/m^3 \cdot s$)

$\Gamma_{g,eq}$ = vapor generation rate in the thermal equilibrium model ($kg/m^3 \cdot s$)

Δl = characteristic length for subcooled boiling, $\Delta l = \lambda_{eq} - \lambda_1$ (m)

Δp = pressure drop (MPa)

$\Delta \rho$ = density difference between liquid and vapor at saturation (kg/m^3)

δ = perturbation

λ_1 = boiling boundary (m)

λ_{eq} = boiling boundary in the thermal equilibrium model (m)

ν = specific volume (m^3/kg)

ρ = coolant density (kg/m^3)

Ω_1 = two-phase mixture phase change frequency, $\Omega_1 = \dfrac{v_{fg}}{h_{fg}} \dfrac{q'' P_h}{A_c}$ (rad/s)

Subscripts

eq = thermal equilibrium

exit = channel outlet

f = saturated liquid

fg = difference between values of vapor and liquid at saturation

g = saturated vapor

i = axial node number

in = channel inlet

m = two-phase mixture

nod = lower nonheating part

nou = upper nonheating part

ori = orifice

λ = properties at net vapor generation point

ACKNOWLEDGMENT

The authors extend their deepest appreciation to M. S. Kazimi at Massachusetts Institute of Technology and P. Saha at General Electric Company for their enormous support, suggestions, and help in this work.

REFERENCES

1. M. ISHII, "Thermally Induced Flow Instabilities in Two-Phase Mixtures in Thermal Equilibrium," PhD Thesis, School of Mechanical Engineering, Georgia Institute of Technology (1971).

2. J. ZHAO, P. SAHA, and M. S. KAZIMI, "Hot-Channel Stability of Supercritical Water-Cooled Reactors—I: Steady-State and Sliding Pressure Startup," *Nucl. Technol.*, **158**, 158 (2007).

3. P. SAHA, "Thermally Induced Two-Phase Flow Instabilities, Including the Effect of Thermal Non-Equilibrium Between the Phases," PhD Thesis, School of Mechanical Engineering, Georgia Institute of Technology (1974).

4. M. Z. PODOWSKI, "Modeling and Analysis of Two-Phase Flow Instabilities," *Proc. 10th Int. Topl. Mtg. Nuclear Reactor Thermal Hydraulics (NURETH-10)*, Seoul, Korea, October 5–9, 2003.

5. A. DOKHANE et al., "Nuclear-Coupled Thermal-Hydraulic Nonlinear Stability Analysis Using a Novel BWR Reduced Order Model: Part 1—The Effects Using Drift Flux Versus Homogenous Equilibrium Models," *Proc. 11th Int. Conf. Nuclear Engineering (ICONE-11)*, Tokyo, Japan, April 20–23, 2003.

6. J. ZHAO, P. SAHA, and M. S. KAZIMI, "Hot-Channel Stability of Supercritical Water-Cooled Reactors—II: Effect of Water Rod Heating and Comparison with BWR Stability," *Nucl. Technol.*, **158**, 174 (2007).

7. W. AMBROSINI, "On the Analogies in the Dynamic Behaviour of Heated Channels," *Nucl. Eng. Des.*, **237**, 1164 (2007).

8. D. BESTION, "The Physical Closure Laws in the CATHARE Code," *Nucl. Eng. Des.*, **124**, 229 (1990).

9. P. CODDINGTON and R. MACIAN, "A Study of the Performance of Void Fraction Correlations Used in the Context of Drift-Flux Two-Phase Flow Models," *Nucl. Eng. Des.*, **215**, 199 (2002).

10. S. LEVY, "Forced Convection Subcooled Boiling-Prediction of Vapor Volumetric Fraction," *Int. J. Heat Mass Transfer*, **10**, 951 (1967).

11. N. E. TODREAS and M. S. KAZIMI, *Nuclear System I, Thermal Hydraulic Fundamentals*, Chap. 9, Hemisphere Publishing Corporation (1990).

12. P. SAHA and N. ZUBER, "An Analytical Study of Thermally Induced Two-Phase Flow Instabilities Including the Effect of Thermal Non-Equilibrium," *Int. J. Heat Mass Transfer*, **21**, 415 (1978).

13. M. ISHII and N. ZUBER, "Thermally Induced Flow Instabilities in Two Phase Mixtures," *Proc. 4th Int. Heat Transfer Conf.*, Paris, France (1970).

14. J. ZHAO, C. P. TSO, and K. J. TSENG, "SCWR Single Channel Stability Analysis Using a Response Matrix Method," *Nucl. Eng. Des.*, **241**, 7, 2528 (2011).

15. M. B. CARVER, "An Analytical Model for the Prediction of Hydro-Dynamic Instability in Parallel Heated Channels," Report No. 2681, Atomic Energy Canada Limited (1968).

16. K. SOLBERG, "Resulats des Essais d'Instabilites sur la Boucle 'Culine' et Comparisons avec un Code de Cakcyk," Note 225, Centre d'Etudes Nucleaires de Grenoble (1966).